The 4th International Symposium on More Electric Aircraft Technology (MEA 2017)

8–9 November 2017

Research on inter-turn short circuit of armature windings in the multiphase synchronous generator–rectifier system

Yuguang Sun, Shanming Wang, Ziguo Huang, Shujun Mu

State Key Laboratory of Control and Simulation of Power System and Generation Equipment, Department of Electrical Engineering, Tsinghua University, Beijing 100084, People's Republic of China
E-mail: wangsm96@mails.tsinghua.edu.cn

Published in *The Journal of Engineering*; Received on 11th February 2018; Accepted on 15th February 2018

Abstract: The multiphase synchronous generator–rectifier system could provide an ideal DC power source for more electric aircraft (MEA). When the inter-turn short-circuit fault occurs in phase windings of the generator, a large short-circuit current would be introduced inside the armature windings, which could cause severe damages to the system for overheat in the windings and irons as well as huge electromagnetic forces on the end coils. To improve the reliability of the MEA, this study researches on the inter-turn fault of the multiphase generator–rectifier system, including the theoretical analysis, numerical simulation and experimental verification. A 12-phase system is taken for example, and a multi-loop mathematical model is built up to calculate all voltages and currents in the multiphase synchronous generator–rectifier system with armature inter-turn fault. Many factors are thoroughly considered in the model, including the location and short-turns of fault, space harmonics of air-gap magnetic field and the changing circuit topology of the system. The mathematical model is verified by fault experiment results. Moreover, the electric characteristics of the fault are summarised, which could provide a quantitative basis for early detection of the inter-turn faults in the multiphase generator–rectifier system.

1 Introduction

The more electric aircraft (MEA) has greatly increased the overall performances of the aircraft, for use of electricity instead of centralised hydraulic energy and pressure energy [1]. As a result of more usage of electricity, the aircraft requires a high-quality power source, especially for the DC power source. The multiphase generator–rectifier system could provide an ideal DC power source for MEA, due to its advantages in smaller ripple in output DC voltage, smaller electromagnetic interference, higher power density, higher efficiency and higher reliability [2–5]. As the safe operation is of primary importance to the aircrafts, this paper researches on the characteristics and detection of the common faults in the multiphase generator–rectifier systems.

Presently, researches on the external faults of the multiphase generator–rectifier systems mainly include some kinds of asymmetric terminal short circuit on the AC side in no-load condition [6], the sudden short circuit on the DC side [7], the open circuit of the switches in bridge rectifiers [8, 9] and so on. For the winding internal fault, studies show that inter-turn short circuit in the stator may introduce a larger short-circuit current inside the ordinary three-phase synchronous generator, which would cause severe damages to the system for the overheat in the windings and the irons as well as the huge electromagnetic forces on the end coils and huge electromagnetic forces. If not handled in time, the inter-turn faults might deteriorate into phase-to-phase short circuit known as more destructive fault [10]. Similarly, this kind of inter-turn short circuit fault may also occur in the armature windings of the multiphase generator–rectifier systems, which are more complicated and seldom researched before.

A 12-phase system is taken for example in the paper. For calculation of the fault characteristic, a detailed multi-loop mathematical model of the multiphase generator–rectifier system with armature inter-turn short circuit fault is built up. Based on the data obtained from experiment and simulation on the 12-phase machine, electrical characteristics of the fault are extracted, which would be useful to the fault damage assessment and fault detection in the armature of multiphase machine that is applied in the generator–rectifier system.

2 Mathematical model

A 12-phase generator–rectifier system is taken as a general example. As shown in Fig. 1, the stator windings of the 12-phase generator are constructed with four Y-connection three-phase windings, displaced in turn by 15° (electrical angle).

To the 12-phase generator–rectifier system shown in Fig. 1, the circuit topology of conducting loops, which consists of stator phases, switching devices and load on the DC side is changed periodically with the on-and-off states of the switches. Different from the common three-phase generator, phase currents of the multiphase generator are non-sinusoidal and contain time-harmonic components even under normal condition, due to non-linear effects result from the switching devices.

Lots of works have been done to model and analyse the generators with bridge rectifiers. The AC phase voltages are usually assumed to be symmetrical sinusoidal under normal condition [11, 12]. However, under the internal short-circuit fault the voltage assumptions are not suitable because of distortion of the phase voltages in the generator. In a three-phase generator–rectifier system, the connection matrix method is used to deal with the relationship among the generator, the bridge rectifier and the DC load [13, 14].

In this paper, the multi-loop method is adopted to calculate the inductance parameters so as to take the distortion of air-gap magnetic field after the internal fault [10, 15] into consideration. Besides,

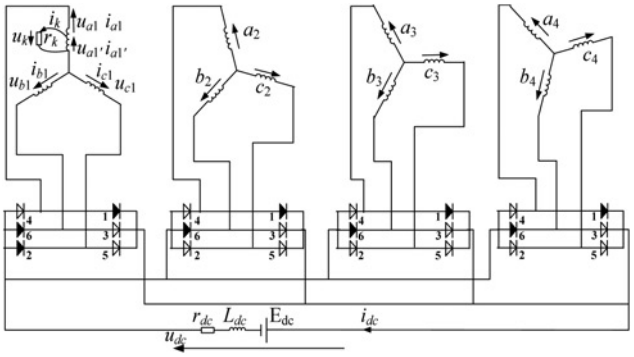

Fig. 1 *Schematic diagram of the armature inter-turn short circuit in the 12-phase generator rectifier system*

the connection matrix method is extended for the multiphase rectifier system with armature inter-turn short circuit.

2.1 Voltage equations

The referential direction for voltages, currents and flux linkages is set as follows: positive current excites positive flux linkage. For the rotor loops (including field loop and damper loops), the motor-reference convention for the relation between voltages and currents is used. For the stator loops, the generator-reference convention for the relation between voltages and currents is used.

2.1.1 Voltage equation of rotor loops: The rotor loop voltage equations of the 12-phase generator–rectifier system are similar to those in ordinary three-phase synchronous generator [10]. The loop voltage equation of field winding is

$$u_{fd} = p\psi_{fd} + r_{fd} i_{fd} \tag{1}$$

where u_{fd}, ψ_{fd} and r_{fd} are voltage, flux linkage and resistance of the field winding, respectively. p is the differential operator, i.e. d/dt.

For the damper windings, the practical mesh circuit of damper loops is shown in Fig. 2. The voltage equation of damper loop Di is

$$\begin{aligned} 0 &= p\psi_{\mathrm{D}i} + r_{\mathrm{D}i} i_{\mathrm{D}i} - (r_{c,i-1} i_{\mathrm{D},i-1} + r_{c,i-1} i_{\mathrm{D},i+1}) \\ &\quad (i = 1, 2, \ldots, d) \end{aligned} \tag{2}$$

where d is the total number of damper bars; $\psi_{\mathrm{D}i}$ and $r_{\mathrm{D}i}$ are flux linkage and resistance of damper loop Di, respectively; r_{ci} is the resistance of damper bar; and r_{ei} is end-ring resistance; so $r_{\mathrm{D}i} = r_{ci} + r_{c,\,i+1} + 2r_{ei}$.

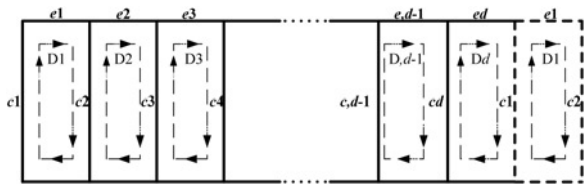

Fig. 2 *Damper loops*

So the voltage equations of all the rotor loops could be assembled into matrix form as follows:

$$\begin{bmatrix} u_{fd} \\ 0 \\ 0 \\ 0 \\ \vdots \\ 0 \\ 0 \end{bmatrix} = p \begin{bmatrix} \psi_{fd} \\ \psi_{\mathrm{D}1} \\ \psi_{\mathrm{D}2} \\ \psi_{\mathrm{D}3} \\ \vdots \\ \psi_{\mathrm{D},d-1} \\ \psi_{\mathrm{D}d} \end{bmatrix}$$

$$+ \begin{bmatrix} r_{fd} & & & & & & & \\ & r_{\mathrm{D}1} & -r_{c2} & & & & -r_{c1} & \\ & -r_{c2} & r_{\mathrm{D}2} & -r_{c3} & & & & \\ & & -r_{c3} & r_{\mathrm{D}3} & -r_{c4} & & & \\ & & & & \ddots & & & \\ & & & & -r_{c,d-1} & r_{\mathrm{D},d-1} & -r_{cd} & \\ & & & & & -r_{cd} & r_{\mathrm{D}d} & \end{bmatrix} \begin{bmatrix} i_{fd} \\ i_{\mathrm{D}1} \\ i_{\mathrm{D}2} \\ i_{\mathrm{D}3} \\ \vdots \\ i_{\mathrm{D},d-1} \\ i_{\mathrm{D}d} \end{bmatrix}$$

$$= p \begin{bmatrix} \psi_{fd} \\ \boldsymbol{\psi}_d \end{bmatrix} + \begin{bmatrix} r_{fd} & \\ & \boldsymbol{r}_d \end{bmatrix} \begin{bmatrix} i_{fd} \\ \boldsymbol{I}_d \end{bmatrix} \tag{3}$$

2.1.2 Voltage equations of stator windings and DC load: In order to set up the voltage equations of the stator, each normal phase, such as $b1$ and $c1$ shown in Fig. 1, is considered as a component. The faulted phase is considered to be split into two components. Taking phase $a1$ in Fig. 1 for example, in case of the inter-turn short-circuit fault, $a1$ is separated into two components, fault phase $a1$ and additional fault phase $a1'$.

Windings from the short-circuit point to the terminal are regarded as fault phase $a1$, and windings from the neutral point to the short-circuit point is regarded as the additional fault phase $a1'$. Besides, the short-circuit line k shown in Fig. 1 is also regarded as an additional component, where r_k is the resistance of line k. So there are 14 stator components' voltage equations, which can be assembled into matrix form as follows:

$$\begin{bmatrix} u_{a1} \\ u_{b1} \\ \vdots \\ u_{c4} \\ u_{a1'} \\ u_k \end{bmatrix} = p \begin{bmatrix} \psi_{a1} \\ \psi_{b1} \\ \vdots \\ \psi_{c4} \\ \psi_{a1'} \\ \psi_k \end{bmatrix} + \begin{bmatrix} r_{a1} & & & & & \\ & r_{b1} & & & & \\ & & \ddots & & & \\ & & & r_{c4} & & \\ & & & & r_{a1'} & \\ & & & & & r_k \end{bmatrix} \cdot \begin{bmatrix} i_{a1} \\ i_{b1} \\ \vdots \\ i_{c4} \\ i_{a1'} \\ i_k \end{bmatrix} \tag{4}$$

where u, i, ψ and r are the voltage, current, flux linkage and resistance of all components, respectively. While the subscripts $a1$, $b1$,…, k represent the different components. Especially, the flux linkage of short circuit line k is 0.

The voltage equation of DC load is

$$u_{\mathrm{dc}} = L_{\mathrm{dc}} \cdot p i_{\mathrm{dc}} + r_{\mathrm{dc}} i_{\mathrm{dc}} + E_{\mathrm{dc}} \tag{5}$$

where u_{dc}, i_{dc}, L_{dc} and r_{dc} are the voltage, current, inductance and resistance of the DC load, respectively. E_{dc} represents the counter electromotive force (EMF).

doi: 10.1049/joe.2018.0026

Based on the voltage equations of all the components, the voltage equations in the matrix form could be assembled

$$\boldsymbol{U} = p\boldsymbol{\psi} + \boldsymbol{RI} + \boldsymbol{E} \tag{6}$$

where $\boldsymbol{U}$, $\boldsymbol{I}$, $\boldsymbol{\psi}$ and $\boldsymbol{E}$ accordingly represent voltages, currents, flux linkages and counter EMF of these components

$$\boldsymbol{U} = \begin{bmatrix} u_{fd} & \mathbf{0}^{\mathrm{T}} & u_{a1} & u_{b1} & \cdots & u_{c4} & u_{a1'} & u_k & u_{\mathrm{dc}} \end{bmatrix}^{\mathrm{T}} \tag{7}$$

$$\boldsymbol{I} = \begin{bmatrix} i_{fd} & \boldsymbol{I}_d^{\mathrm{T}} & i_{a1} & i_{b1} & \cdots & i_{c4} & i_{a1'} & i_k & i_{\mathrm{dc}} \end{bmatrix}^{\mathrm{T}} \tag{8}$$

$$\boldsymbol{\psi} = \begin{bmatrix} \psi_{fd} & \boldsymbol{\psi}_d^{\mathrm{T}} & \psi_{a1} & \psi_{b1} & \cdots & \psi_{c4} & \psi_{a1'} & 0 & L_{\mathrm{dc}} i_{\mathrm{dc}} \end{bmatrix}^{\mathrm{T}} \tag{9}$$

$$\boldsymbol{E} = \begin{bmatrix} 0 & \cdots & 0 & E_{\mathrm{dc}} \end{bmatrix}^{\mathrm{T}} \tag{10}$$

The resistance matrix is

$$\boldsymbol{R} = \mathrm{diag}\begin{pmatrix} r_{fd} & \boldsymbol{r}_d & r_{a1} & r_{b1} & \cdots & r_{c4} & r_{a1'} & r_k & r_{\mathrm{dc}} \end{pmatrix} \tag{11}$$

The flux linkage can be calculated by

$$\boldsymbol{\psi} = \boldsymbol{MI} \tag{12}$$

where the inductance matrix $\boldsymbol{M}$ is

$$\boldsymbol{M} = \begin{bmatrix} L_{fd} & \boldsymbol{M}_{fd,d} & M_{fd,a1} & \cdots & M_{fd,c4} & M_{fd,a1'} & 0 & 0 \\ \boldsymbol{M}_{d,fd} & \boldsymbol{L}_d & \boldsymbol{M}_{d,a1} & \cdots & \boldsymbol{M}_{d,c4} & \boldsymbol{M}_{d,a1'} & \mathbf{0} & \mathbf{0} \\ M_{a1,fd} & \boldsymbol{M}_{a1,d} & L_{a1} & \cdots & M_{a1,c4} & M_{a1,a1'} & 0 & 0 \\ \vdots & \vdots & \vdots & \ddots & \vdots & \vdots & \vdots & \vdots \\ M_{c4,fd} & \boldsymbol{M}_{c4,d} & M_{c4,a1} & \cdots & L_{c4} & M_{c4,a1'} & 0 & 0 \\ M_{a1',fd} & \boldsymbol{M}_{a1',d} & M_{a1',a1} & \cdots & M_{a1',c4} & L_{a1'} & 0 & 0 \\ 0 & \mathbf{0}^{\mathrm{T}} & 0 & \cdots & 0 & 0 & 0 & 0 \\ 0 & \mathbf{0}^{\mathrm{T}} & 0 & \cdots & 0 & 0 & 0 & L_{\mathrm{dc}} \end{bmatrix} \tag{13}$$

where L is self-inductance and M is mutual inductance. The next-to-last row and column of the inductance matrix $\boldsymbol{M}$, representing the inductances related with the short-circuit line k, values are all 0.

Based on the multi-loop method, all inductance parameters of the loops and components in matrix $\boldsymbol{M}$ can be calculated under the armature internal fault condition [10].

2.2 State equations of all loop currents

In (6), the voltages of the rotor loops are known, while the voltages of stator windings and DC load are unknown. Therefore, (6) is unsolvable. The voltage equations of these components should be transformed into loop voltage equations so that they could be solved.

Circuit topology of the conducting stator loops changes along with the on-and-off state of the switches in the generator–rectifier system. With a connection matrix of the system named $\boldsymbol{T}$, (6) can be transformed into the state equations. The element in the matrix is 1 if the related component is in the loop and has the same reference directions with the loop. If the reference directions of the component are opposite to the loop, the related element in the matrix is −1. The element in the matrix is 0 if the related component has no relationship with the loop. At certain instant shown in Fig. 1, the diode drawn solid is switched on, and that drawn hollow is switched off. The connection matrix $\boldsymbol{T}$ is expressed as (14).

In the connection matrix $\boldsymbol{T}$, each column corresponds to a component which is labelled on the top of the matrix, and each row represents a loop. The d in the row number represents the number of damper loops. The first $d+1$ rows are the voltage equations of the rotor loops, which do not need to be transformed. Row $d+2$ to row $d+6$ of $\boldsymbol{T}$ represent the normal conducting loops through each bridge rectifiers, and row $d+7$ represents the additional short circuit loop.

Based on the connection matrix $\boldsymbol{T}$, the loop voltage equations could then be achieved from the components voltage (6):

$$\boldsymbol{U}' = \boldsymbol{T} \cdot p\boldsymbol{\psi} + \boldsymbol{TRI} + \boldsymbol{TE} \tag{15}$$

Equation (15) is solvable since the voltage column vector of the stator loops $\boldsymbol{U}'$ is known. In the 12-phase generator–rectifier system with the inter-turn short circuit fault shown in Fig. 1, the voltage column vector $\boldsymbol{U}'$ is

$$\boldsymbol{U}' = \begin{bmatrix} u_{fd} & \mathbf{0}^{\mathrm{T}} & -2\Delta u & -2\Delta u & -2\Delta u & -2\Delta u & -2\Delta u & 0 \end{bmatrix}^{\mathrm{T}} \tag{16}$$

where Δu represents the conduction voltage drop of the diode.

The mathematic relation between the currents of all components as $\boldsymbol{I}$ and those of the stator loops as $\boldsymbol{I}'$ is

$$\boldsymbol{I} = \boldsymbol{T}^{\mathrm{T}} \boldsymbol{I}' \tag{17}$$

where $\boldsymbol{T}^{\mathrm{T}}$ is the transposed matrix of $\boldsymbol{T}$.

Substituting (12) and (17) into (15), the state equations of loop currents could be obtained as follows:

$$\begin{aligned} \boldsymbol{U}' &= \boldsymbol{TU} \\ &= \boldsymbol{TMT}^{\mathrm{T}} p\boldsymbol{I}' + \boldsymbol{T}\begin{pmatrix} p\boldsymbol{M} + \boldsymbol{R} \end{pmatrix}\boldsymbol{T}^{\mathrm{T}} \boldsymbol{I}' + \boldsymbol{TE} \end{aligned} \tag{18}$$

The state equation (18) could be solved by the numerical method. Then all currents in the system, such as field current, currents of the normal loops and the short-circuit turns in armature windings, could be obtained.

2.3 Diode turn-on and turn-off criterion and simulation process

Once the currents and voltages of the stator windings and DC load are calculated, the existing operation state of the bridge rectifier

$$\boldsymbol{T} = \begin{array}{c} \begin{matrix} fd & d & a1 & b1 & c1 & a2 & b2 & c2 & a3 & b3 & c3 & a4 & b4 & c4 & a1' & k & \mathrm{dc} \end{matrix} \\ \begin{bmatrix} 1 & & & & & & & & & & & & & & & & \\ & \boldsymbol{I} & & & & & & & & & & & & & & & \\ & & 1 & 0 & -1 & & & & & & & & & & 1 & & 1 \\ & & 1 & -1 & 0 & & & & & & & & & & 1 & & 1 \\ & & & & & 1 & -1 & 0 & & & & & & & & & 1 \\ & & & & & & & & 1 & -1 & 0 & & & & & & 1 \\ & & & & & & & & & & & 1 & -1 & 0 & & & 1 \\ & & & & & & & & & & & & & & 1 & 1 & \end{bmatrix} \end{array} \begin{array}{c} \mathrm{row} \\ 1 \\ \vdots \\ d+2 \\ d+3 \\ d+4 \\ d+5 \\ d+6 \\ d+7 \end{array} \tag{14}$$

doi: 10.1049/joe.2018.0026

could be determined sequentially. In the multiphase generator–rectifier system, the commutation process is more complicated than that in common three-phase system. It contains the process not only among the switches of the same rectifier, but also among different rectifiers.

The turn-off criterion is very simple. Once the phase current reduces from positive to negative, the corresponding switch is considered as turn-off.

The turn-on criterion is a little complex, since the four-group three-phase windings have their own neutral points and the neutral points are independent. The diode is turned on or not is determined by the difference between the line voltages inside each three-phase windings and the DC voltage. If the relative line voltage becomes larger than the DC voltage, the diode turns on, otherwise the diode keeps off.

The occurrence of the armature inter-turn fault would not change the above on-and-off criterion of the switches. With these criterions, the operation state of the bridge rectifier is obtained. Sequentially, connection matrix $\boldsymbol{T}$ and state equation (18) would be adjusted for the next step, and then the next currents and voltages could be obtained. Iterating these procedures, the steady-state and transient currents of all the loops could be solved, whether under normal or fault conditions.

3 Experiment and simulation

To test the validity of the mathematical model, a 12-phase model machine was used for the experiment and simulation. The armature internal fault can be realised artificially on the model machine, in which several extra taps inside the 12-phase windings are led out except for the general terminal taps.

The setup of the internal fault experiments is shown in Fig. 3. In the experiments, the four-pole model machine is driven to the constant speed of 1500 r/min by an asynchronous motor. The load on the DC side is a resistance, so E_{dc}, i.e. the counter EMF of the DC load shown in Fig. 1, is 0. The voltages and currents of the stator and field windings as well as the DC load are recorded by the oscillograph.

This paper takes the metallic inter-turn fault experiment as an example, in which the short circuit occurred between 25% and the neutral of $a1$ phase, with a resistance load $r_{\mathrm{dc}} = 0.62\ \Omega$ on the DC side. In this experiment, the field current i_{fd} is reduced to 1.01 A to avoid damage of the machine for the overlarge short circuit current. The experiment and simulation waveforms of the currents before and after the fault are shown in Figs. 4–7 in per-unit value. The base value of the short-circuit current is equal to the root-mean-square value of the phase current in normal operation under rated field current condition with the load resistance $r_{\mathrm{dc}} = 0.62\ \Omega$.

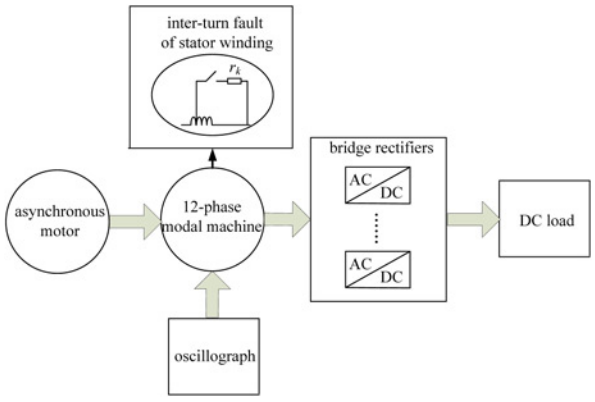

Fig. 3 *Schematic diagram of experiment platform*

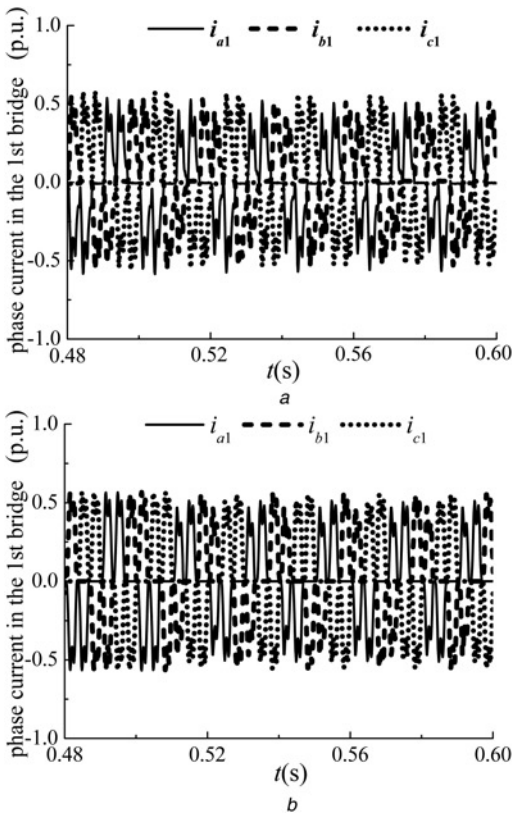

Fig. 4 *Current waveforms of the first group of three-phase windings in the 12-phase model machine before and after the short circuit of 25% of a1 phase under $r_{dc} = 0.62\ \Omega$ resistive load condition*
a Experiment current waveforms
b Simulation current waveforms

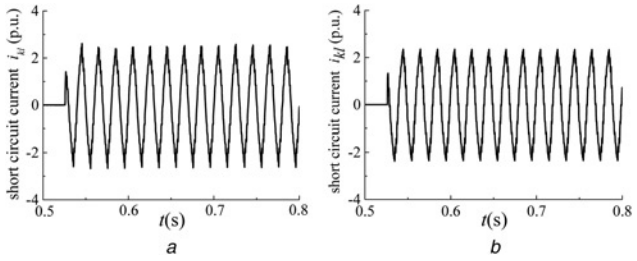

Fig. 5 *Current waveforms of the short-circuit loop before and after the short circuit of 25% of a1 phase under $r_{dc} = 0.62\ \Omega$ resistive load condition*
a Experiment current waveform
b Simulation current waveform

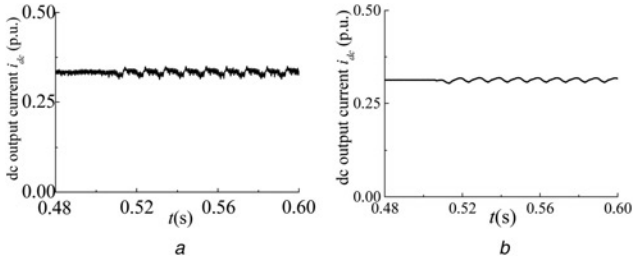

Fig. 6 *Current waveforms of the DC load before and after the short circuit of 25% of a1 phase under $r_{dc} = 0.62\ \Omega$ resistive load condition*
a Experiment current waveform
b Simulation current waveform

doi: 10.1049/joe.2018.0026

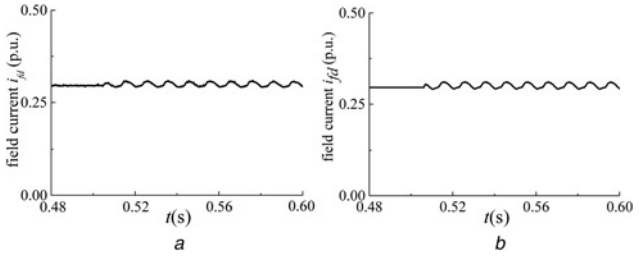

Fig. 7 *Waveforms of the field current before and after the short circuit of 25% of a1 phase under $r_{dc} = 0.62\ \Omega$ resistive load condition*
a Experiment current waveform
b Simulation current waveform

The above waveforms show that the experiment and simulation results coincide well with each other. In order to give further verification to the accuracy of the computation result, the harmonic analysis of the AC and DC components of the steady-state currents is obtained as shown in Table 1.

Table 1 shows that the calculation errors of the steady-state currents are almost within 20%, compared with the experiment results. It should be noted that the third harmonic current of $a1$ phase in the experiment results under normal operation is caused by the manufacturing error.

The simulation and experiment results coincide well with each other, which confirm the accuracy of the mathematical model and simulation method. Furthermore, the mathematical model is not only applicable for the 12-phase generator–rectifier system, but also for other multiphase systems with certain groups of Y-connected windings.

4 Inter-turn fault characteristics

In order to present the fault characteristics more clearly, Figs. 8–10 are given which take the amplitude spectrum to show variation of the currents of faulted phase $a1$, the non-fault phase $b1$ and the short-circuit loop k based on the simulation results.

Figs. 8 and 9 show that both of the phase currents decrease in the inter-turn fault, while the changes on the current of faulted phase $a1$ are more obvious than that of the non-fault phase $b1$. The current of

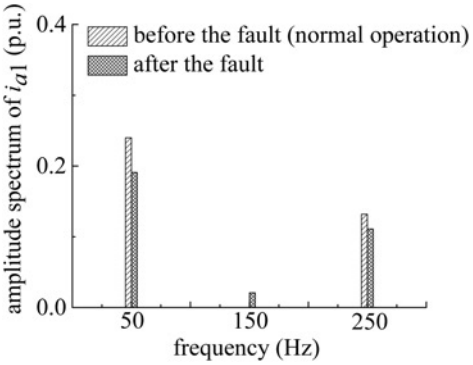

Fig. 8 *Current amplitude spectrum of the faulted phase a1 before and after the inter-turn short-circuit fault*

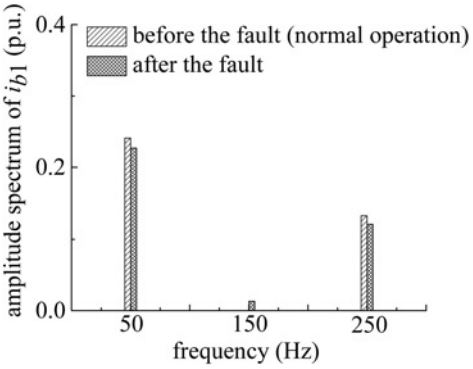

Fig. 9 *Current amplitude spectrum of the non-fault phase b1 before and after the inter-turn short-circuit fault*

the additional fault phase $a1'$ increases a lot attributed to the large current of short-circuit loop shown in Fig. 10.

Based on the harmonic analysis of fault currents in the third section, the characteristics of the armature inter-turn short-circuit

Table 1 Harmonic analysis of steady-state currents of the 12-phase machine before and after the inter-turn short circuit of 25% of $a1$ phase under $r_{dc} = 0.62\ \Omega$ resistive load condition

		Before fault			After fault (during steady state)		
		Experiment results	Simulation results	Calculation error, %	Experiment results	Simulation results	Calculation error, %
harmonic effective values of current in $a1$ phase	fundamental	0.231	0.240	4.3	0.184	0.191	3.7
	3rd	0.003	0	—	0.026	0.021	−21.5
	5th	0.109	0.132	20.7	0.093	0.111	18.3
harmonic effective values of current in $b1$ phase	fundamental	0.240	0.241	0.4	0.228	0.227	−0.6
	3rd	0.004	0	—	0.010	0.013	25.5
	5th	0.115	0.133	15.2	0.106	0.121	13.9
harmonic effective values of current in $c1$ phase	fundamental	0.230	0.240	4.7	0.195	0.207	6.3
	3rd	0.007	0	—	0.036	0.032	−9.8
	5th	0.108	0.134	24.5	0.084	0.099	18.4
harmonic effective values of short-circuit current	fundamental	0	0	—	1.538	1.482	−3.7
	3rd	0	0	—	0.059	0.068	16.0
	5th	0	0	—	0.063	0.047	−25.5
harmonic effective values of DC output current	DC	0.333	0.313	−6.1	0.329	0.312	−5.2
	2nd	0.000	0.000	—	0.004	0.003	−11.6
	24th	0.004	0.000	—	0.004	0.003	−28.3
harmonic effective values of field current	DC	0.296	0.296	0.0	0.296	0.299	1.1
	2nd	0.000	0	—	0.000	0.000	—
	4th	0.000	0	—	0.005	0.006	21.8

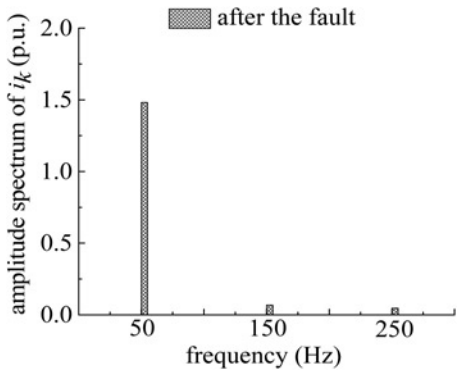

Fig. 10 *Current amplitude spectrum of the short-circuit loop, before and after the inter-turn short-circuit fault*

fault of the 12-phase generator–rectifier system are summarised as follows:

(i) The phase currents decrease, and the third harmonic which does not exist under normal condition appears in the phase currents when the inter-turn short circuit occurs.
(ii) The current of the short circuit loop and the additional fault phase are large that would be harmful to the generator. These fault currents mainly contain fundamental and other odd-order harmonics, including the third harmonic.
(iii) Besides the DC component, the field current contains the second and other even-order harmonics.
(iv) Besides the DC component and 24th harmonic, the output current of the rectifier to the DC load contains the second and other even-order harmonics.

Due to the asymmetry in line voltages of the 12-phase windings after faults, some other harmonics except for the 24th harmonic appear in the output DC voltage of the rectifier. The DC voltage is of even symmetry since any line voltages are of odd symmetry. The DC voltage contains only the second and other even-order harmonics, and there will be no fundamental and other odd-order harmonics theoretically. Accordingly, the output current has the same harmonic characteristic.

5 Conclusions

By means of the multi-loop theory, this paper establishes the mathematical model of the multiphase synchronous generator with rectifier loads under armature inter-turn fault. The steady-state and transient currents and voltages are obtained before and after the inter-turn faults. The validity of the mathematical model is confirmed by a series of experiments on a 12-phase model machine. The fault characteristics of the armature inter-turn short-circuit in the 12-phase generator–rectifier system are concluded.

With the help of the mathematical mode, the short-circuit current and other electrical quantities can be predicted, which may be useful to explore the fault detection of the inter-turn short circuits in the multiphase generator–rectifier system.

6 Acknowledgment

This work was supported by the National Natural Science Foundation of China (no. 51277103). Their assistance is gratefully acknowledged.

7 References

[1] Hirst M., McLoughlin A., Norman P.J., *ET AL.*: 'Demonstrating the more electric enigine: a step towards the power optimised aircraft', *IET Electr. Power Appl.*, 2011, **5**, pp. 3–13
[2] Levi E.: 'Multiphase electric machines for variable-speed applications', *IEEE Trans. Ind. Electron.*, 2008, **55**, (5), pp. 1893–1909
[3] Parsa L.: 'On advantages of multiphase machines'. IEEE Industrial Electrical Conf., 6 November 2005, pp. 1574–1579
[4] Jordan S., Apsley J.: 'Diode rectification of multiphase synchronous generators for aircraft applications [C]'. Energy Conversion Congress and Exposition. IEEE, 2011, pp. 3208–3215
[5] Todd R., Forsyth A.J.: 'DC-bus power quality for UAV systems during generator fault conditions'. 5th IET Int. Conf. on Power Electronics, Machines and Drives, 2010, pp. 1–6
[6] Ma W., Hu A., Wang L.: '12-phase rectifier fault diagnosis based on voltage waveform analysis', *Trans. China Electrotech. Soc.*, 1997, **12**, (6), pp. 49–54
[7] Zhang Q., Lu G., Zhang C.: 'Simulated study of the multiple cascade medium-voltage inverter based on PSCAD/EMTDC [C]'. 2016 19th Int. Conf. on Electrical Machines and Systems (ICEMS). IEEE, 2016, pp. 1–6
[8] Jordan S., Apsley J.: 'Open-circuit fault analysis of diode rectified multiphase synchronous generators for DC aircraft power systems'. 2013 IEEE Int. Electric Machines & Drives Conf. (IEMDC), May 2013, pp. 926–932
[9] Huang Z., Sun Y., Wang S., *ET AL.*: 'Analysis and diagnosis on open-circuit fault of diode rectifier in 12-phase synchronous generator system [C]'. European Conf. on Power Electronics and Applications. IEEE, 2014, pp. 1–9
[10] Wang X.H., Chen S., Wang W., *ET AL.*: 'A study of armature winding internal faults for turbo generators', *IEEE Trans. Ind. Appl.*, 2002, **38**, (3), pp. 625–631
[11] Alt J.T., Sudhoff S.D., Ladd B.E.: 'Analysis and average-value modeling of an inductorless synchronous machine load commutated converter system', *IEEE Trans. Energy Convers.*, 1999, **14**, (1), pp. 37–43
[12] Sudhoff S.D., Corzine K.A., Hegner H.J., *ET AL.*: 'Transient and dynamic average-value modeling of synchronous machine fed load-commutated converters', *IEEE Trans. Energy Convers.*, 1996, **11**, (3), pp. 508–514
[13] Williamson S., Volschenk A.F.: 'Time-stepping finite element analysis for a synchronous generator feeding a rectifier load', *IEE Proc. Electr. Power Appl.*, 1995, **142**, (1), pp. 50–56
[14] Wang S., Wang X., Li Y.: 'Steady-state performance of synchronous generators with AC and DC stator connections considering saturation', *IEEE Trans. Energy Convers.*, 2002, **17**, (2), pp. 176–182
[15] Gao J.D., Zhang L.Z., Wang X.H.: 'AC machine systems' (Tsinghua University Press, Beijing, 2009) (Springer-Verlag Berlin, Heidelberg)